

Entanglement phase transitions in measurement-only dynamics

Matteo Ippoliti,¹ Michael J. Gullans,² Sarang Gopalakrishnan,^{3, 4} David A. Huse,^{2, 5} and Vedika Khemani¹

¹*Department of Physics, Stanford University, Stanford, CA 94305, USA*

²*Department of Physics, Princeton University, Princeton, NJ 08544, USA*

³*Department of Engineering Science and Physics,
CUNY College of Staten Island, Staten Island, NY 10314, USA*

⁴*Initiative for Theoretical Sciences, The Graduate Center, CUNY, New York, NY 10016, USA*

⁵*Institute for Advanced Study, Princeton, NJ 08540, USA*

Unitary circuits subject to repeated projective measurements can undergo an entanglement transition as a function of the measurement rate. This transition is generally understood in terms of a competition between scrambling due to unitary dynamics and the disentangling effects of measurements. We find that, surprisingly, entanglement transitions are possible even in the absence of scrambling unitary dynamics. We illustrate this phenomenon in models where the unitary dynamics is non-scrambling, as well as for systems in which the dynamics is entirely due to local few-site measurements. This opens the door to a vast landscape of measurement-only models, in which the ‘‘scrambling’’ and ‘‘un-scrambling’’ effects that drive the entanglement transition are not separable into distinct physical processes. We show numerical results on the entanglement phase diagrams, critical points, and locality properties of some of these measurement-only models. We find that an entangling (volume-law) phase is the default outcome, while disentangling (area-law) phases are possible in the presence of special restrictions on the size or commutativity of the measurements. We propose *frustration* of the measurement ensemble as the principle driving the entanglement transition in this class of dynamics.

I. INTRODUCTION

The study of out-of-equilibrium quantum dynamics is an exciting research frontier¹. Many important developments have pushed this frontier forward in recent years, especially in regards to the dynamics of isolated quantum systems. Among these developments are many-body localization (MBL)^{2–4}, quantum chaos^{5,6}, many-body ‘‘quantum scars’’^{7–10}, and the discovery of non-equilibrium Floquet phases^{11,12}. Many of these developments were born of a cross-fertilization between the sub-fields of quantum information theory, quantum gravity and condensed matter theory, with the dynamics of quantum entanglement serving as a unifying thread in systems ranging from electrons in solids to cold atomic gases to black holes^{13–25}. Our understanding of even fundamental questions pertaining to the out-of-equilibrium dynamics of many-body systems is still nascent, and the development of new models and tools for tackling these forms a major research enterprise. In this context, *random unitary circuits* have emerged as a versatile tool for the study of many-body dynamics in various contexts^{22,26–31}.

The increased focus on quantum dynamics is also motivated by the advent of ‘‘noisy, intermediate-scale quantum’’ (NISQ) devices³². While an ideal quantum computer (or simulator) is a closed, unitarily-evolving system, any realistic implementation will have both controlled operations and unintended interactions with its environment, leading to non-unitary, open-system dynamics. In a fully fault-tolerant quantum computer such imperfections can be handled blindly, by means of quantum error correction. On the other hand, in NISQ devices the quantum dynamics of the hardware cannot be decoupled from the information-processing task at hand, and

thus must be benchmarked accurately. To wit, Google’s recent demonstration of ‘quantum supremacy’³³ turned on comparing probability distributions drawn from an ideal random unitary circuit and a real, noisy one. A very different context for open-system dynamics involves quantum gravity, namely black hole evaporation and the information paradox, where entanglement between the black hole interior and outer Hawking radiation modes plays a crucial role (for a recent review see Ref. 34). Here, too, random circuits have proven to be a useful tool^{35–37}.

An open system is generically described by a mixed state; characterizing entanglement in mixed states is a challenging problem in general³⁸. However, in specific cases, dissipation can freeze a system in a pure state, e.g., via the quantum Zeno effect and its many-body generalizations^{39–43}. Recent works have approached this question from a novel perspective: instead of studying the steady state of the system plus its environment, they have focused on entanglement dynamics along *single quantum trajectories*^{44,45}. In the framework of quantum trajectories, one models the system-environment interaction as a sequence of projective measurements acting on the system; each measurement collapses the system’s wavefunction with a random outcome determined by the Born probabilities, so the system is always in a pure state (of decreasing norm). Refs. 46–49 explored the dynamics of the simplest such model, in which the intrinsic dynamics of the system is given by a random unitary circuit, and is interleaved with projective measurements acting on single sites. Surprisingly, these systems exhibit a phase transition in the entanglement structure of single trajectories, as a function of the measurement rate. This ‘‘entanglement transition’’ separates a disentangling phase, where the entanglement entropy S obeys an area-

law, and an entangling phase, where it obeys a volume-law. Intuitively, as frequent strong measurements entangle the system to an environment, monogamy⁵⁰ prevents different parts of the system from becoming entangled with each other.

This is a rather surprising result. It conflicts with the intuition that quantum coherence is a delicate resource, unstable to the decohering effects of an environment. Moreover, while entanglement takes a long time to build up and propagate, it can seemingly be destroyed globally by a single measurement. A very useful perspective on the transition, which clarifies how these issues are sidestepped, is achieved by thinking in terms of quantum information scrambling^{51,52}: chaotic unitary dynamics tends to hide quantum information in highly nonlocal correlations that are inaccessible to local measurements. Local measurements then do not learn much about the state of the system (this is related to the fact that random unitary circuits are good at encoding quantum information^{35,53}). Additionally, a complementary view of these phenomena is that of *purification* (rather than entanglement) phases and transitions^{54–56}, where the volume- and area-law phases differ in their ability to purify an initial mixed state. In the area-law phase, an initially mixed state is purified after a number of measurements that is polynomial in system size (so measurements are able to efficiently extract information about the initial state), whereas in the volume-law phase the initial state stays mixed for exponentially longer timescales. The persistence of a mixed subspace corresponds to the spontaneous formation of a quantum error correcting code capable of protecting encoded qubits from the measurements. However, due to the simultaneous action of scrambling and “unscrambling” dynamics in unitary-projective circuits, the precise mechanism underlying this code formation process remains poorly understood.

In light of this, it is natural to ask just *how* scrambling the unitary evolution must be to obtain a volume law phase. A physically relevant case where this question may be probed is MBL, where both information scrambling and entanglement dynamics are logarithmically slow in time^{57–62}. One might think that this scrambling is too slow to compete with measurements performed at a finite rate, leading generically to an area-law phase. Surprisingly, we find evidence to the contrary, even in models where the unitary dynamics is strictly non-scrambling (rather than slowly scrambling) – i.e. the combination of non-scrambling unitaries and unscrambling measurements can somehow still furnish a volume law phase!

Building on this, we show how these non-scrambling models can equivalently be seen as featuring *measurement-only dynamics*, where the unitary gates are discarded altogether, at the expense of introducing multi-site (but still local) measurements. Such measurement-only dynamics is characterized by the ensemble of operators that one is allowed to measure on the system, which can in turn be specified by various

parameters. Varying these, we are able to obtain and characterize entanglement phases and phase transitions.

Unlike the unitary-projective case where the balance between scrambling and unscrambling is naturally controlled by the measurement rate p , in the measurement-only case it is not *a priori* clear which parameters determine the entangling properties of the dynamics. Multi-site measurements evidently can both scramble *and* unscramble quantum information at the same time. While the issue of quantifying the net balance between these coexisting tendencies is still unsolved, we find that a crucial role is played by the ‘frustration’ of the measurement ensemble, an idea we make more precise below which roughly coincides with the degree of mutual incompatibility (anticommutativity) between different measurements. The essential point is as follows: if one measures two commuting operators, one acquires two bits of information about the state of the system, whereas if one measures two noncommuting operators, the second measurement scrambles the information about the state that the first measurement provided.

Aside from the entanglement transitions, the measurement-only dynamics we study in this work has other interesting properties. The volume-law phase is especially remarkable; its existence means that acting repeatedly with a certain set of measurements can endow the steady state with resistance *against the same set of measurements*, thus defining a sort of self-generated quantum code. Another interesting aspect of the measurement-only dynamics relates to locality: formulating sensible notions of locality and causality becomes challenging when measurements, with their ‘spooky action at a distance’ effects, are allowed. We take initial steps in addressing these questions in this type of dynamics.

On the experimental side it is plausible to imagine platforms where few-site projective measurements may be easier to implement than a universal quantum computing gate set. In particular, the ability to implement *a single type* of multi-site Pauli measurement combined with single-qubit Clifford gates would suffice to explore a wide variety of models. This may make measurement-only dynamics a more practical alternative to unitary-projective dynamics in some near-term quantum simulators.

Finally, we remark on some connections between this work and other topics in quantum information theory involving measurements. While it is known that measurements possess the same computational power as quantum gates⁶³, this resource-theoretic equivalence relies on specific protocols, or structured sequences of measurements. The dynamics we study, on the contrary, features *spatiotemporally random* sequences of measurements. It is thus crucial to distinguish the matter-of-principle, resource-theoretic possibility of certain outcomes from their realization in a stochastic setting. We also remark on the distinction between this measurement-only dynamics and measurement-based quantum computing (MBQC)⁶⁴: in MBQC one is handed an entangled re-

source state and, by performing measurements in a specific sequence, obtains the (classical) answer to a pre-defined computational problem, at the expense of destroying the resource state. In contrast to MBQC, the measurement-only dynamics we study does not rely on initial resources, is spatiotemporally random, and produces highly entangled states as its output.

The paper is organized as follows. In Sec II we consider the question of entanglement transitions with non-scrambling, MBL-inspired unitary circuits and projective measurements. This motivates the introduction of dynamics in measurement-only models (MOMs), which we define in more generality in Sec. III. In Sec. IV we show numerical results for the entanglement phase diagrams in several MOMs. Critical points in these same models are discussed in Sec. V. Sec. VI focuses on the locality and causality structure of measurement-only dynamics. We conclude by summarizing our results and pointing to open questions and future directions in Sec. VII.

II. MOTIVATION: “MEASUREMENT-ENABLED ENTANGLEMENT” IN l -BIT CIRCUITS

As mentioned above, an appealing interpretation of the entanglement phase transitions in unitary-projective dynamics is based on the competition between the scrambling effect of unitary dynamics and the “unscrambling” effect of local measurements. Measurements tend to degrade locally-accessible quantum information into classical bits, while chaotic unitary dynamics tends to scramble, i.e. hide quantum information in nonlocal degrees of freedom, where it cannot be accessed by local projective measurements. One measure of scrambling in closed quantum systems is furnished by the spread of operators in the Heisenberg picture, captured quantitatively by the out-of-time-ordered correlators (OTOCs)⁶⁵. It is thus tempting to conjecture that the phase of the system is decided by which process happens faster – the information hiding due to the unitary dynamics or the read-out induced by the measurements. Such a scenario naturally yields a critical measurement rate p_c below which the system’s steady state has volume-law entanglement. This scenario also suggests that by tuning the scrambling rate to zero, one should be able to push p_c down to zero. As we will now see, this is not the case.

A. Removing scrambling: l -bit models

To test the above scenario, we consider what happens when the unitary dynamics does *not* scramble at a finite rate. The many-body localized phase provides an example. Here, entanglement is known to grow only logarithmically in time upon quenching from an unentangled product state^{15,66}. Slow scrambling can be explained using the l -bit representation of a fully-MBL Hamiltonian^{67–69},

$$H_{\text{MBL}} = \sum_i h_i \tau_i^z + \sum_{k \geq 2} \sum_{i_1 < \dots < i_k} J_{i_1, \dots, i_k} \tau_{i_1}^z \cdots \tau_{i_k}^z \quad (1)$$

where the τ_i^z operators are local integrals of motion (l -bits) and the couplings decay exponentially with distance, $J_{i, \dots, j} < e^{-|i-j|/\xi}$. In such a system, the only mechanism for the production of entanglement is dephasing between different l -bit basis states. Two l -bits separated by a distance r become aware of each other only after a time $\sim e^{r/\xi}$ (when the exponentially small coupling J between them has had enough time to induce significant dephasing). It follows that the entanglement entropy grows as $O(\ln t)$ and that, likewise, local operators spread within a logarithmic ‘light cone’.

We now ask whether interspersing the above dynamics with local projective measurements yields an entanglement transition. Based on the scenario we outlined earlier, we expect the answer would be negative – for any rate $p > 0$, the read-out of information is presumably faster than the scrambling. However, surprisingly, we still find an entanglement phase transition even for such a ‘slowly scrambling’ model, provided the axis along which the spin is measured has a component orthogonal to the l -bit direction!

To address this question further, we focus on an even less entangling model of unitary dynamics – in Eq. (1), we only allow two-body couplings out to a *finite* distance n . This cut-off gets rid of scrambling altogether, capping the amount of entanglement to an $O(n)$ size-independent (hence area-law) value, if one starts from a non-entangled initial product state. Moreover, to facilitate numerical simulations, we consider a Clifford circuit model with two gates: the two-qubit controlled- Z gate $\text{CZ}_{ij} = e^{-i\frac{\pi}{4}(Z_i-1)(Z_j-1)}$ ($i < j < i+n$) and the single-qubit phase-gate $P_i = e^{-i\frac{\pi}{4}Z_i}$. The system is subject to a layer of unitaries,

$$U_{l\text{-bit}} = \prod_i P_i^{a_i} \prod_{i < j < i+n} \text{CZ}_{ij}^{b_{ij}}, \quad (2)$$

with $a_i, b_{ij} \in \{0, 1\}$ chosen randomly with probability $1/2$ (notice all the gates commute so there is no need to specify the order in which they act). Then, for each site, we either measure X , measure Z , or do not perform any measurement, with probabilities p_x , p_z and $1 - p_x - p_z$ respectively. The whole process is iterated until a steady-state value of entanglement is reached. This setup is illustrated in Fig. 1.

Notice that Z measurements create distentangled l -bits which commute with the unitary dynamics; the only way a measured l -bit can again become entangled with the rest of the system is by being measured in the X direction first. Hence the dynamics with $p_x = 0$ and $p_z > 0$ trivially leads to a product state as soon as every site is measured once. Measuring in the X basis, thus breaking the conservation law, is necessary to obtain any nontrivial steady state.

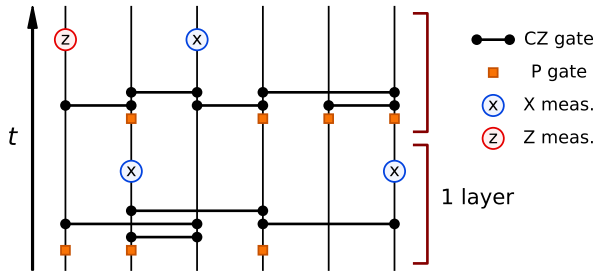


FIG. 1. Schematic of the l -bit circuit with projective measurements. This circuit has $n = 3$: CZ gates are allowed between qubits i, j with $|i - j| < 3$, i.e. nearest and next-nearest neighbors. All allowed gates happen with probability $1/2$ in each layer.

Surprisingly, we find that the above model (which, to reiterate, has area-law entanglement at both $p_x = 0$ and $p_x = 1$) admits a volume-law phase. Fig. 2(a) shows the phase boundary in the p_x, p_z plane for the model with range $n = 4$ (CZ gates between nearest, next-nearest and third-nearest neighbors). For $0 < p_x \lesssim 0.7$ the model is in a volume-law phase which is robust to sufficiently infrequent Z measurements. A similar picture holds for all $n > 3$, with an increasingly robust volume-law phase, see Fig. 2(b). The data include fractional values of $n = n^* + \epsilon$ (with $n^* \in \mathbb{N}$, $0 < \epsilon < 1$). These are defined as having a CZ gate between qubits i, j in each unitary layer with probability $1/2$ if $|i - j| < n^*$ and $\epsilon/2$ if $|i - j| = n^*$, so that for $\epsilon \rightarrow 1$ one recovers the definition in Eq. (2) with $n = n^* + 1$. Considering now measurements in the X basis only ($p_z = 0$) we find that the model with $n = 3$ is area-law for any p_x . A volume-law phase is present for $n > 3.1$ – though precise determination of the critical n requires taking $p_x \rightarrow 0^+$ which is problematic. We shall return to this point from a different perspective in Sec. IV B.

A few comments are in order. First, this result shows that an interpretation of entanglement transitions in unitary-projective circuits based on the competition between the rates of measurement and unitary scrambling is incomplete: entanglement transitions are possible even with a scrambling rate of zero. Second, the result does not follow trivially from the fact that the X measurements break the conservation laws in the unitary part of the circuit ($[\mathcal{U}_{l\text{-bit}}, Z_i] = 0$). While clearly necessary, this condition is insufficient – e.g., the models discussed above with $n \leq 3$ remain area-law despite the integrals of motion being broken by measurements. Finally, it is remarkable that the interplay of two ingredients that are separately incapable of creating much or any entanglement (the finite-range l -bit gates and the single-site measurements) can nonetheless yield a volume-law phase. This phenomenon, which can be called “measurement-enabled entanglement”, necessitates a new framework. In the rest of the article we advance the proposal that such a frame-

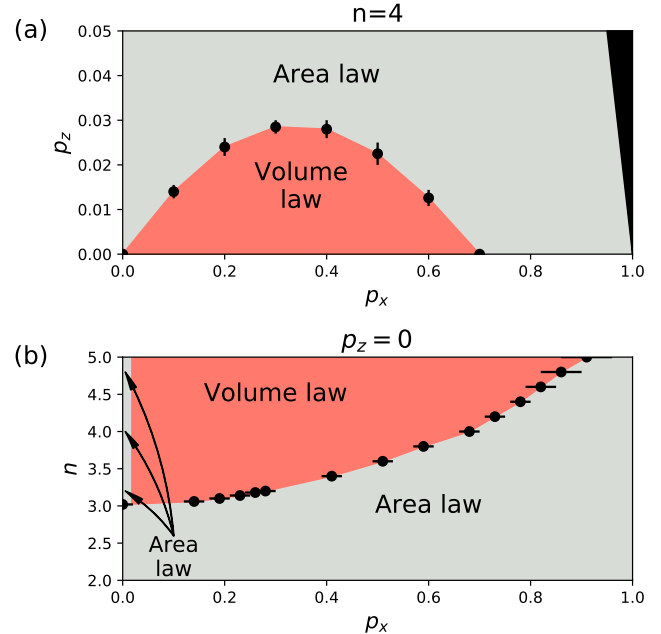


FIG. 2. Entanglement phase diagram of the l -bit unitary-projective dynamics as a function of range n and probabilities p_x, p_z of projective measurements in the X and Z basis. (a) Fixed range $n = 4$. For $0 < p_x \lesssim 0.7$ there is a volume-law phase robust to the introduction of sufficiently infrequent Z measurements. (b) Measurements in the X basis only ($p_z = 0$). A volume-law phase exists for $n > 3.03$. The $p_x = 0$ line is always area-law, regardless of n .

work relies on measurements alone.

B. Removing unitary gates: measurement-only models

Let us take a Pauli string O and denote the projective measurement of O by μ_O :

$$\mu_O |\psi\rangle = \frac{(\mathbb{I} + sO) |\psi\rangle}{\|(\mathbb{I} + sO) |\psi\rangle\|},$$

where $s \in \{+1, -1\}$ is picked randomly according to the usual Born probability, $\text{Prob}(s) = \frac{1}{2}(1 + s \langle \psi | O | \psi \rangle)$. It is clear from the above definition that the following holds for any unitary U :

$$\mu_O U = U \mu_{U^\dagger O U}. \quad (3)$$

A consequence of this fact, unique to non-scrambling circuits, is that the l -bit unitary-projective circuit discussed above can be entirely separated into a unitary part and a projective part that are both local: taking a layer of l -bit gates Eq. (2) past an X measurement according to Eq. (3) yields an operator with finite support. Specifically, since $\text{CZ}_{ij}^\dagger X_i \text{CZ}_{ij} = X_i Z_j$ and $\text{P}_i^\dagger X_i \text{P}_i = Y_i$ (as

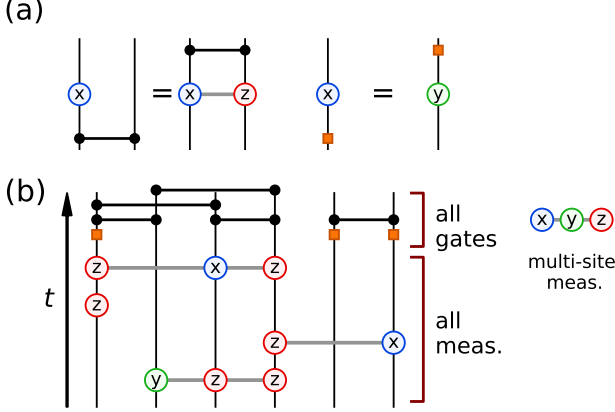


FIG. 3. (a) Rules for taking CZ and P gates past single-site X measurements, Eq. (3). (b) The l -bit circuit from Fig. 1 after taking all the gates past the measurements. Each single-site X measurement develops “tails” of Z operators on either side of maximum length $n - 1$ (2 in this case) due to conjugation by CZ gates.

sketched in Fig. 3(a)), we have

$$U_{l\text{-bit}}^\dagger X_i U_{l\text{-bit}} = X_i (-iZ_i)^{a_i} \prod_{\substack{|i-j| < n \\ j \neq i}} (Z_j)^{b_{ij}} \quad (4)$$

which is a Pauli string of length at most $2n - 1$, characterized by an X or Y operator surrounded by finite “tails” of \mathbb{I} or Z operators on both sides. Notice that even when conjugating by several layers of $U_{l\text{-bit}}$, the operator can’t grow any longer than that – the only effect is to change the values of a_i and b_{ij} . After taking all the unitary layers to the end of time, $t = T$, we are left with a circuit consisting purely of local multi-site measurements drawn from some finite ensemble of Pauli strings, as in Eq. (15), followed by a final layer of unitaries (see Fig. 3(b) for an example with $T = 2$ layers). This final layer, despite being the composition of T layers, is in fact equivalent to a single layer having $a_i^{\text{tot}} = \sum_{t=1}^T a_i(t)$ and $b_{ij}^{\text{tot}} = \sum_{t=1}^T b_{ij}(t)$ modulo 2 (which are still uniformly distributed binary numbers). Therefore it can change the entanglement about any given bond by at most $n - 1$ bits, and cannot change the entanglement phase of the steady state (area-law to volume-law or *vice versa*), and thus can be safely discarded for our purposes. This leaves us with a circuit consisting exclusively of local measurements of multi-site Pauli strings.

It follows that the entanglement transition in l -bit unitary-projective circuits discussed earlier can actually be understood as the result of projective measurements alone. This type of quantum dynamics, known as measurement-induced dynamics, has been considered in the context of quantum information processing and metrology^{70–72} while its entanglement properties are largely unexplored. From the result above it follows that

measurements can play both sides in the competition underlying entanglement transitions – at the same time degrading quantum information to classical bits *and* hiding quantum information from local, accessible degrees of freedom into non-local, inaccessible ones. This has the potential to either increase *or* decrease the complexity of the state.

As we have seen above, entanglement phase transitions are possible in this type of dynamics. In the following we introduce a broader class of measurement-only models, including and generalizing the l -bit model discussed above, and begin the study of their entanglement properties.

III. MEASUREMENT-ONLY DYNAMICS

A. Setup

We define measurement-only dynamics by introducing an ‘ensemble’ $\mathcal{E} = (P_\alpha, \{O_\alpha\})$, consisting of a set of Pauli strings O_α and a probability distribution P_α over $\{O_\alpha\}$. Any such ensemble \mathcal{E} induces a random dynamics in the following way: at each time step, an O_α is picked according to P_α and measured on the system; doing so updates the state according to the ‘wavefunction collapse’ $|\psi_{t+1}\rangle = \mu_{O_\alpha} |\psi_t\rangle$; starting from an initially non-entangled product state, this step is iterated until a steady-state distribution of the entanglement over the so-generated ensemble of quantum trajectories and circuits is achieved. Note that general multi-site measurements are known to be universal for quantum computation⁶³; the Pauli measurements considered here have the same computational power as Clifford gates. This ensures that highly-entangled states may be produced, at least as a matter of principle.

In order to sensibly define phases of matter, some additional requirements are needed. In particular, we assume:

- (i) Locality. We assume the system consists of L qubits arranged on a 1D chain; each Pauli string $\{O_\alpha\}$ is supported in an interval of length r (the ‘range’ of the ensemble) which does not scale with system size.
- (ii) Statistical translational invariance. Setting $\tilde{L} = L + 1 - r$ (L) for open (periodic) boundary conditions, we assume the ensemble is of the form $\mathcal{E} = (P_\alpha U_i, \{O_{\alpha,i}\})$, with $i \in \{0, \dots, \tilde{L} - 1\}$ labelling spatial displacements, $U_i = 1/\tilde{L}$ the uniform distribution, and $O_{\alpha,i} = T_i O_\alpha T_i^\dagger$ the translation by i sites of a Pauli string O_α supported on sites $\{1, \dots, r\}$.

Measurement ensembles are thus specified by a range r and a probability distribution over $(4^r - 1)$ Pauli strings (measuring the identity is equivalent to not doing any measurement). Throughout the following, we are going to assume the above restrictions and lighten the no-

tation by denoting the translationally invariant ensemble $(P_\alpha U_i, \{O_{\alpha,i}\})$ simply by $(P_\alpha, \{O_\alpha\})$. α thus labels ‘species’ of Pauli strings, and the random spatial location i is implicit. In addition, we redefine time as $t = m/L$ where m is the number of measurements that have been performed. With this convention, each site is on average measured of order once per unit time and the thermodynamic limit is well-defined.

We emphasize that the assumption of translation invariance applies to the probability distribution underlying the dynamics. Individual realizations of the dynamics will be random in space, as well as time. Measurements arranged in regular spatiotemporal patterns may give rise to different phenomena; we leave this direction to future work.

B. Measurements in the stabilizer formalism

We briefly summarize the update rules for measuring Pauli strings on stabilizer states as they will help in building intuition about measurement-only dynamics. A more thorough review is offered in Appendix A.

A stabilizer state is a state of the form

$$\rho = \frac{1}{2^{L-s}} \prod_{i=1}^s \frac{\mathbb{I} + g_i}{2}, \quad (5)$$

where the $\{g_i\}$ are commuting Pauli strings called the stabilizer generators. If $s = L$ the state is pure, $\rho = |\psi\rangle\langle\psi|$, with $|\psi\rangle$ the unique simultaneous +1 eigenvector of all the g_i ’s; $r < L$ represents a mixed state. Expressing the generators as products of Pauli X and Z operators (up to a phase) defines a ‘stabilizer tableau’ \mathcal{T} via

$$g_i = \prod_n X_n^{\mathcal{T}_{i,2n}} Z_n^{\mathcal{T}_{i,2n+1}} \quad (6)$$

Measuring a Pauli string O on a state like Eq. (5) has several possible outcomes, discussed in detail in Appendix A, that are qualitatively different. In particular, the purity of a mixed state (Eq. (5) with $s < L$) changes as follows: if O commutes with all g_i ’s and does not already belong to the stabilizer group, it gets added as a new generator and the purity increases, $s \mapsto s + 1$; otherwise the purity is unchanged. In all cases, O itself is a stabilizer after the measurement is performed. This in general requires a redefinition of the other stabilizer generators to ensure commutation with O .

C. Simple limits

To gain some intuition about measurement-only stabilizer dynamics, we begin by considering two extreme limits: (i) the ensemble of L single-site Z_i operators, and (ii) the ensemble of $(4^L - 1)$ global Pauli strings other than the global identity, with operators picked from

a uniform distribution in both cases. The former has range $r = 1$ and only one species $O_\alpha = Z$; the latter has range $r = L$ (which violates the assumption of locality) and $(4^L - 1)$ distinct species corresponding to all possible Pauli strings. Let us adopt the purification perspective⁵⁴ to analyze these examples: we start from a maximally mixed state $\rho \propto \mathbb{I}$, measure strings from the ensemble, and decide whether the state purifies in $\log(L)$ time (‘pure phase’, equivalent to the area-law entanglement phase) or remains mixed out to exponentially long times (‘mixed phase’, equivalent to the volume-law entanglement phase).

In case (i) the system trivially reaches a pure product state in the Z_i computational basis as soon as every site has been measured once, which takes $O(L \ln L)$ measurements and thus belongs to the pure, or area-law, phase. Unsurprisingly, single-site measurements are purely disentangling.

In case (ii), the first measurement (starting from the identity state, i.e. the empty tableau) always adds one row, g_1 , and thus one bit of purity. The second measurement is equally likely to commute or anticommute with g_1 : it thus takes two attempts, on average, to add a second row g_2 . Adding g_3 to the tableau takes on average 4 attempts, and so on – the purification time scales exponentially with L , and thus the dynamics is in the mixed phase. This is also not surprising as the strings are completely nonlocal and all-to-all.

What is not clear from these simple examples is whether it is possible to achieve a volume-law phase by measuring *short* Pauli strings (of finite range $r \gtrsim 1$). In this case, the first $O(L)$ measurements are likely to commute, partially purifying the initial state; however, subsequent measurements past this point might either commute or anticommute with previous measurements. Thus a volume law phase where the system stops purifying can occur. Whether this happens in practice is not obvious: while it is known that arbitrary states can be produced via measurements only⁶³, this relies on very special protocols (e.g. gate teleportation⁷³ or entanglement swapping⁷⁴). It is not immediately obvious whether a volume-law entangled phase can be generated by measurements placed *randomly* in space and time. This situation is reminiscent of the entanglement transition in unitary-projective circuits: while it is immediately clear in that case that both volume- and area-law entangled states can be constructed (e.g. in the trivial limits of measurement probabilities $p = 0$ and $p = 1$), it is not obvious, and was indeed a surprising result, that these extreme limits should extend to *phases* separated by a sharp transition at some critical value $0 < p_c < 1$.

In the present case of measurement-only dynamics, how to interpolate between the limits considered above is not as clear: there is no unique knob to tune (like the measurement probability p in unitary-projective circuits), but rather a huge, multi-dimensional landscape of possible measurement ensembles; with trivial exceptions like the ones examined above, these ensembles are

not straightforwardly sorted from ‘‘more entangling’’ to ‘‘more disentangling’’. Understanding this measurement-only dynamics in some generality thus requires an organizing principle. In the following, we propose and explore a potential organizing principle: the degree of ‘‘frustration’’ of the measurement ensemble.

D. Measurement frustration

As we just discussed, fully commuting ensembles of measurements invariably ‘‘localize’’ the wave function in a simultaneous eigenstate, which is area-law entangled if the measurements are local. Some level of non-commutativity among measurements in the ensemble is thus necessary to produce an entangling phase. Non-commuting observables cannot, by definition, be known at the same time; the wave function thus cannot satisfy all the measurements in the ensemble at once. We refer to this inability to satisfy non-commuting measurements as ‘frustration’⁷⁵. It is tempting to conjecture that a suitably defined ‘degree of frustration’ (a function of the O_α and P_α) could predict the steady-state entanglement phase of a given ensemble (without resorting to explicit simulation of finite-size dynamics).

To this end, it is helpful to introduce the *frustration graph* of an ensemble of Pauli measurements^{75–78}. This is a graph whose vertices represent all the operators in the ensemble $\{O_{\alpha,i}\}$, and where two vertices are connected by an edge if and only if the corresponding operators anticommute. The adjacency matrix of this graph is also known as the frustration matrix. In our case, translation invariance imposes a quasi-1D structure to the frustration graph, and we can define a frustration *tensor* as

$$\Gamma_\ell^{\alpha\beta} = O_{\alpha,i} \circ O_{\beta,i+\ell}, \quad (7)$$

where $A \circ B \in \mathbb{Z}_2$ is a ‘symplectic product’ defined to be 0 if A and B commute, 1 otherwise. In Eq. (7) we have split the species and spatial indices and taken advantage of translation invariance to express Γ as a function of the displacement ℓ only. A direct consequence of the definition is the symmetry $\Gamma_\ell^{\alpha\beta} = \Gamma_{-\ell}^{\beta\alpha}$. The frustration graph, or its associated tensor, also define an ‘effective range’, \tilde{r} , as the minimum displacement $\ell > 0$ such that $\Gamma_\ell^{\alpha\beta} = 0$ for all species α, β . This obeys $\tilde{r} \leq r$ where r is the range as defined earlier, i.e. the maximum spatial extent of the Pauli strings in the ensemble (non-overlapping strings must necessarily commute). However there are cases where the inequality is strict, $\tilde{r} < r$, e.g. the l -bit ensemble to which we return in Sec. IV B.

The Γ tensor captures crucial information about the dynamics; in particular we show in Appendix B that under mild additional assumptions it is sufficient to simulate the dynamics and thus determine the entanglement (or purification) phase. Graph-theoretic properties or invariants may place constraints on (or pose obstructions to) the existence of an entangling phase in a given ensemble, regardless of the probabilities P_α . We return to this

in Sec. IV C, where we discuss a result in this spirit on bipartite graphs.

In cases where the probability distribution P_α is not uniform, it must be taken into account as well in order to formulate a quantitative description of measurement frustration. The simplest step in this direction is represented by the averaged frustration tensor:

$$\bar{\Gamma}_\ell = P_\alpha P_\beta \Gamma_\ell^{\alpha\beta}. \quad (8)$$

We call this quantity the ‘frustration profile’ of the ensemble. It is the probability that two random measurements displaced by ℓ anticommute. This can be a useful heuristic, as we show in the next Section. However the averaging gets rid of important information, and ensembles with the same $\bar{\Gamma}$ (but different Γ) can belong to different entanglement phases.

IV. MEASUREMENT ENSEMBLES

A. Factorizable ensembles

The dynamics introduced in the previous Section, even under assumptions of locality and translation invariance, produces a wide parameter space of models – a hypothetical entanglement phase diagram on range- r models would be $O(4^r)$ -dimensional, which is prohibitive already for $r = 2$. At the same time most of these dimensions are likely unimportant. It is thus crucial to find ways to describe generic measurement ensembles with few parameters. One way to achieve this is to consider ‘factorizable’ ensembles, which we now define.

1. Definition

We call an ensemble ‘factorizable’ if it consists of Pauli strings (of a fixed length r) that are distributed according to some underlying *single-site* distribution, i.e. if

$$O_\alpha = \bigotimes_{n=1}^r \sigma_{\alpha_n} \implies P_\alpha = \prod_{n=1}^r q_{\alpha_n} \quad (9)$$

where α is a string of Pauli matrix labels $\alpha_n \in \{\mathbb{I}, X, Y, Z\}$ and q is a probability distribution over the four single-site Pauli matrices. This structure reduces the space of models from $O(4^r)$ dimensions to just three dimensions – the single-site q_X , q_Y and q_Z probabilities, which live in a tetrahedron, $0 \leq q_X + q_Y + q_Z \leq 1$. Dropping the identity (which tends to increase commutativity, thus likely pushing the dynamics towards area law entanglement) further reduces the phase diagram to the triangle $q_X + q_Y + q_Z = 1$.

While these ensembles still include exponentially many species, which make the frustration graph or tensor cumbersome, it is straightforward to calculate the frustration profile $\bar{\Gamma}_\ell$ introduced in Eq. (8). Letting $\mathbf{q} =$

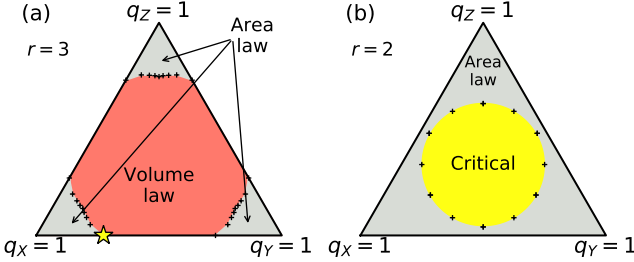


FIG. 4. Phase diagrams of factorizable ensembles $q = (0, q_X, q_Y, q_Z)$ (Pauli strings without identities) for ranges $r = 3$ (a) and $r = 2$ (b). The starred point in (a) is the phase transition studied in Fig. 7. The $+$ symbols are numerical estimates of the phase boundary.

$(q_X, q_Y, q_Z) = \mathbf{q}_\perp + \mathbf{q}_\parallel$, where $\mathbf{q}_\parallel = \frac{1}{3}(1, 1, 1)$ (the center of the triangle) and $\mathbf{q}_\perp \cdot \mathbf{q}_\parallel = 0$, we show in Appendix B that

$$\bar{\Gamma}_\ell = \frac{1}{2} - \frac{1}{2} \left(2q_\perp^2 - \frac{1}{3} \right)^{r-\ell}. \quad (10)$$

The probability of anticommutation for two strings overlapping on a single site, in particular, is

$$\chi \equiv \bar{\Gamma}_{r-1} = \frac{2}{3} - q_\perp^2. \quad (11)$$

2. Entanglement phases for $r \geq 3$

We begin by considering ensembles of the above type, parametrized by the vector of probabilities $\mathbf{q} = (q_X, q_Y, q_Z)$, with range $r = 3$. To reiterate, this ensemble includes all $3^r = 27$ operators of the form $\sigma_a \otimes \sigma_b \otimes \sigma_c$ with $a, b, c \in \{X, Y, Z\}$, picked with probability $q_a q_b q_c$, and measured at a random location in the system. By simulating this model numerically we find that a large part of parameter space belongs to a volume-law entangled phase, see Fig. 4(a). This includes intervals on the sides of the triangular parameter space: e.g. on the $q_Z = 0$ side we have an area-law phase for $q_X < q_{X,c} = 0.274(2)$ and symmetrically $q_X > 1 - q_{X,c}$, while the segment $q_{X,c} < q_X < 1 - q_{X,c}$ is in a volume-law phase. The phase boundary is approximately circular, close to the equal-value contour of the anticommutation probability $\chi \simeq 0.4$.

As the range r of the model is increased, the volume-law phase takes up a progressively larger fraction of the phase diagram. The corners remain trivially area-law for arbitrarily large r , but the extent of the area-law parameter space shrinks. We focus on the $q_Z = 0$ side for simplicity and find that the critical value $q_{X,c}$ obeys

$$r \simeq \frac{k}{2q_{X,c}(1 - q_{X,c})} = \frac{k}{\chi_c} \quad (12)$$

where $k \simeq 1.16$. The critical point for models with long strings ($r \gg 1$) thus occurs at a constant, $O(1)$ value of $r \cdot \chi$. This is suggestive of a balance between the anticommutation probability χ and the range r in determining the entanglement phase: longer Pauli strings generically lead to a volume-law phase, unless they are made to be extremely commuting. More specifically, we note that as $r \rightarrow \infty$, $\chi \rightarrow 0$ along the critical line Eq. (12), the probability of sampling the uniform string made of the majority Pauli, say $Y^{\otimes r}$, is $q_Y^r \simeq (1 - \frac{k}{2r})^r \rightarrow e^{-k/2} \simeq 0.56$. Thus a majority of the measurements are drawn from a set of commuting observables $\{A_j = Y_j \cdots Y_{j+r}\}$, which form a trivial quantum code.

3. $r = 2$: free fermions and criticality

Eq. (12) would suggest that the model with range $r = 2$ should have an entanglement transition at $\chi \simeq 0.58$ (which is lower than the maximal value of $\chi = 2/3$ and thus defines a finite radius q_\perp in parameter space). However, we find no sign of a volume-law phase. Instead, surprisingly, we see evidence of a *critical* phase in a circular region around the center of parameter space, as shown in Fig. 4(b).

Let us start by discussing the sides of the phase diagram, e.g. $q_Z = 0$. The dynamics maps to free-fermions^{79,80}: the Pauli string species

$$\{X_0 X_1, X_0 Y_1, Y_0 X_1, Y_0 Y_1\} \quad (13)$$

are equivalent, under Jordan-Wigner transformation, to

$$\{i\gamma_1\gamma_2, i\gamma_1\gamma_3, i\gamma_0\gamma_2, i\gamma_0\gamma_3\}, \quad (14)$$

where $\gamma_{2j}, \gamma_{2j+1}$ are the two Majorana fermion operators on site j . This property implies that there is a gauge in which each row of the stabilizer tableau \mathcal{T} is a two-Majorana ‘arc’ operator $i\gamma_m\gamma_{m+\ell}$, and one can map the entanglement properties to the distribution of arc lengths $P(\ell)$. A similar model, with two types of operators $\{i\gamma_0\gamma_1, i\gamma_1\gamma_2\}$ (corresponding to spin operators $Z_0, X_0 X_1$), was found to be critical when the two species are measured at the same rate and area-law otherwise, though a mapping to a loop model⁸⁰. The same was also found⁸¹ in a model with operators $\{Z, XZX\}$ (which is equivalent to two copies of $\{Z, XX\}$, as can be seen from their frustration tensors). At the critical point the arc length distribution becomes scale-invariant, $P(\ell) \sim \ell^{-2}$, giving logarithmic entanglement entropy $S(\ell) \sim \ln(\ell)$. This is not seen in the four-operator ensemble of Eq. (14), which is instead in the area-law phase for any value of q_X/q_Y .

The interior of the triangular phase diagram consists of a 9-operator ensemble $\{(X/Y/Z)_0(X/Y/Z)_1\}$ which does not map to free fermions. Numerically we find that the area-law phase identified at the boundary extends in the interior, see Fig. 4(b); however, while we can conclusively rule out a volume-law phase anywhere in the interior, the

system appears to enter a *critical phase* as it approaches the center of the triangle. In this phase, we find that the entanglement entropy diverges logarithmically with system size, $S \sim K \ln \ell$. Though area-to-critical phase boundaries are hard to locate accurately, we find a phase boundary consistent with $\chi \simeq 0.54$ ($q_\perp^2 \simeq 0.13$). Inside the corresponding circular contour, we do not see any signs of saturation in $S(L)$ for sizes up to $L = 512$. We will return to this phenomenology in Sec. IV C.

B. l -bits revisited

1. Ensemble

The l -bit unitary-projective circuits discussed in Sec. II naturally lead to a measurement-only dynamics specified by the ensemble

$$\mathcal{E}_{l\text{-bit}} = \left\{ O_\alpha = X_0 \prod_{\ell=1-n}^{n-1} Z_\ell^{\alpha_\ell} \right\} \quad (15)$$

where $\alpha \in \{0, 1\}^{2n-1}$ labels the operator species (we omit phase factors for simplicity, writing XZ in *lieu* of Y). The uniform probability distribution over the 2^{2n-1} operators is implicit. All operators are characterized by a ‘central site’ that is either a Pauli X or Y , and tails on both sides that are made exclusively of \mathbb{I} or Z Pauli matrices, with equal probability of $1/2$. As written, the above ensembles have range $r = 2n - 1$; however, their frustration profile is $\bar{\Gamma}_\ell = \frac{1}{2}\Theta(n - |\ell|)$, i.e. any two operators displaced by $|\ell| \geq n$ commute, since in that case only their tails (made entirely of \mathbb{I} and Z) overlap. Thus the effective range, as specified by the connectivity of the frustration graph, is $\tilde{r} = n$.

In the factorizable ensemble phase diagrams of Fig. 4, we saw indications that the frustration profile $\bar{\Gamma}$ (Eq. (8)) correlates with the entanglement phase. Here we note that the frustration profile of the l -bit ensemble at $n = 3$ is the ‘box’ $\bar{\Gamma}_\ell = \frac{1}{2}\Theta(3 - |\ell|)$, which coincides with the $r = 3$ factorizable ensemble at the $q_X = q_Y = 1/2$ point. We know (from Sec. II) that the former is in an area-law phase, while the latter was found to be in a volume-law phase (Fig. 4(a)). This example illustrates the fact that the averaged $\bar{\Gamma}_\ell$ (the probability of anticommutation for random measurements displaced by ℓ) does *not* encode enough information to predict the dynamics. The full, species-resolved information in $\Gamma_\ell^{\alpha\beta}$ is necessary.

2. Connection with circuit model

The original unitary-projective l -bit circuit has a measurement rate, p , that (once translated to the measurement-only language) tends to make the measurements more commuting, and thus drives the dynamics towards the area-law phase. In the original circuit, if two

measurements take place in the same time slice within distance n of each other, they manifestly commute; this commutation must be maintained even after getting rid of the CZ gates via the ‘trick’ in Eq. (3). This means that, when switching from the unitary-projective to the measurement-only pictures, an amount of correlation (or memory) is built into the measurements drawn from the ensemble: for instance, after drawing $X_i Z_{i+1}$ one is more likely to draw the commuting observable $Z_i X_{i+1}$ rather than the anticommuting X_{i+1} . In dropping such correlations, we are implicitly taking a $p \rightarrow 0^+$ limit (and concurrently rescaling time, since we are defining one time step as including one measurement, as opposed to the unitary-projective circuit that has Lp measurements per layer). This makes the relation between two models (unitary-projective and measurement-only) a bit subtle. The $p \rightarrow 0^+$ limit more accurately stands for $pL \ll 1$ (very low probability of having two measurements next to each other in the same layer of the original circuit), which is meaningless when taking the thermodynamic limit $L \rightarrow \infty$ first. However, reintroducing the correlations mentioned above can only push the dynamics towards area law, so the measurement-only dynamics provides a strict upper bound to the steady-state entanglement of the hybrid circuit with any finite p .

3. Entanglement transition

As stated in Sec. II, the unitary-projective l -bit dynamics admits a volume-law phase for $n \geq 4$, while $n \leq 3$ is area-law for any measurement rate p . The measurement-only dynamics confirms that result. However, this framework also allows us to smoothly connect the models with ‘range’ n^* and $n^* + 1$ ($n^* \in \mathbb{N}$) via a family of ensembles with fractional $n \equiv n^* + \epsilon$,

$$O_\alpha = X_0 \prod_{\ell=-n^*}^{n^*} Z_\ell^{\alpha_\ell}, \quad P_\alpha = \frac{1}{\mathcal{N}} \epsilon^{\alpha_{-n^*} + \alpha_{n^*}}, \quad (16)$$

where \mathcal{N} is a probability normalization. In other words, Z operators at the extreme points of the tail, $\ell = \pm n^*$, are less frequent than those at other points by a factor of ϵ . The frustration profile of the ensemble in Eq. (16) is

$$\bar{\Gamma}_\ell = \frac{1}{2}\Theta(n^* - |\ell|) + \frac{(2 - \epsilon)\epsilon}{2} \delta_{|\ell|, n^*}.$$

Once $\epsilon = 1$ the bias is gone and we recover the $n = n^* + 1$ ensemble. Taking the parameter ϵ from 0 to 1 interpolates smoothly between $n = n^*$ and $n = n^* + 1$.

We remark that the models with fractional n as defined above are *not* the $p \rightarrow 0^+$ limit of an l -bit unitary-projective circuit with the same fractional value of n , such as those studied in Fig. 2(b). A unitary-projective l -bit circuit with fixed fractional $n = n^* + \epsilon$ ($n^* \in \mathbb{N}$) flows to integer range $n^* + 1$ as $p \rightarrow 0^+$: the measurements rate becomes so low that any CZ gate allowed to happen

in between consecutive measurements will happen with probability 1/2, no matter how low the probability per time step.

When taking n from 3 to 4 in small fractional steps, we encounter an entanglement transition surprisingly close to $n = 3$: the critical point is estimated at $n_c = 3.021(3)$. We emphasize that this critical point is incompatible with $n = 3$, where the dynamics unambiguously converges to an area-law. Nonetheless, proximity to this critical point endows the $n = 3$ l -bit model with a very long correlation length, which could easily be mistaken for critical scaling. The critical properties of this transition are examined in Sec. V.

C. Bipartite ensembles

The ensembles we have considered until now (the factorizable ensembles of Sec. IV A and the l -bit ensembles of Sec. IV B) contain a large number of measurements – exponentially many in the range r . In both cases we have parametrized these large families of measurements with few independent variables, to be able to draw phase diagrams and illustrate the qualitative features driving the transition (range, commutativity of the measurements). We have found that a volume-law phase is the generic outcome for “long enough” and “random enough” Pauli strings – but making these qualifiers more specific remains challenging. In light of this, rather than focusing on what enables a volume-law phase, we take the opposite view of searching for *obstructions* to this generic fate. For this purpose it is most convenient to look at ensembles with few, hand-picked operator species. With few operator species, many properties of the dynamics can be gleaned from the frustration graph. For example, equivalences between ostensibly different ensembles may become apparent, as we discuss in Appendix B.

A case of particular interest is that of ensembles with only two species of operators, $\{A_i, B_i\}$, whose intra-species commutation relations are trivial: $[A_i, A_j] = [B_i, B_j] = 0$. This means the frustration graph is bipartite, i.e. A -type vertices are only connected to B -type vertices, and vice versa. Physically, this situation can describe two quantum error correcting codes whose stabilizers are the $\{A_i\}$ and $\{B_i\}$ respectively. These are mutually incompatible – stabilizers for the A code are interpreted as errors by the B code and vice versa. Both types of operators are measured concurrently with rates proportional to the probabilities P_A, P_B . The phase diagram is thus one-dimensional, parametrized by the bias $\Delta = P_A - P_B$.

The only nontrivial sector in the frustration tensor is $\Gamma_\ell^{AB} = \Gamma_{-\ell}^{BA} \equiv \gamma_\ell$. (We note in passing that any choice for the frustration graph $\gamma \in \mathbb{Z}_2^{2r-1}$ is straightforwardly realized by the ensemble $A_j = X_j, B_j = \prod_\ell Z_\ell^{\gamma_\ell}$.) A spatial reflection $\ell \mapsto -\ell$ implements a species duality transformation $(A, B) \mapsto (B, A), \Delta \mapsto -\Delta$. Since the spatial reflection cannot change the entanglement phase,

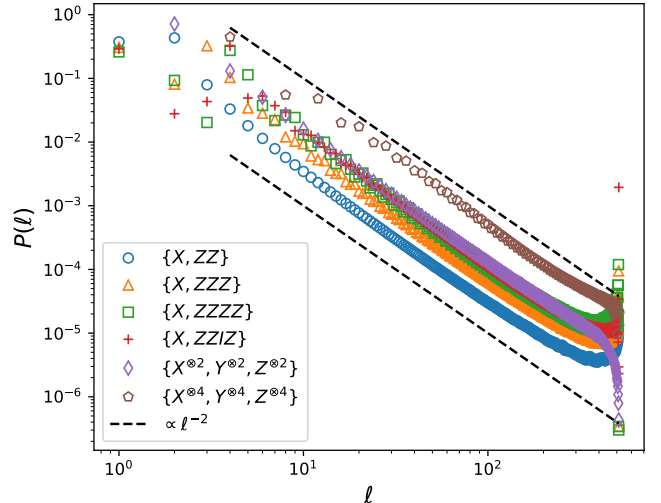


FIG. 5. Probability distribution of stabilizer length $P(l)$ in several bipartite ensembles at the unbiased point $\Delta = 0$ in a system of size $L = 512$ (data aggregated from 10^3 runs for each ensemble). A power-law tail $P(l) \sim l^{-2}$ indicates critical entanglement.

the phase diagram must be symmetric about $\Delta = 0$.

We find, through numerical simulation of all bipartite graphs with effective range $\tilde{r} \leq 6$, that the phase diagram invariably consists of two area-law phases separated by a critical point at $\Delta = 0$ where the distribution of stabilizer lengths obeys $P(l) \sim K l^{-2}$ (see Fig. 5), giving a logarithmically divergent entanglement entropy $S(l) \simeq K \ln(l)$. We note that at least some of these critical points are not proximate to any volume-law phase that we know of, indicating that the physical mechanism for this criticality may be qualitatively different from that of other entanglement transitions in either hybrid circuits or measurement-only models. We also note that this introduces a wide class of entanglement critical points whose position is exactly known and fixed by a duality ($A \leftrightarrow B$), unlike e.g. hybrid circuits where p_c must often be determined numerically. This may provide a useful setting for future studies of the underlying critical theory.

An intuitive picture for these critical points goes as follows. At maximum bias $\Delta = 1$ ($P_B = 0$) the dynamics is fully un-frustrated and projects the state into the A code space (with area-law entanglement). As infrequent B measurements are introduced ($0 < \Delta < 1$) small patches of B code (i.e. intervals in space where $B_x |\psi\rangle = |\psi\rangle$) are constantly created and destroyed over a background of A code. These patches of B code are prevented from spreading beyond some finite length scale by the frequent A measurements. The same, with $A \leftrightarrow B$, is true at $\Delta < 0$. At $\Delta = 0$, however, neither code dominates and the formation of long stabilizers becomes possible.

We compute the stabilizer length distribution $P(l)$ in

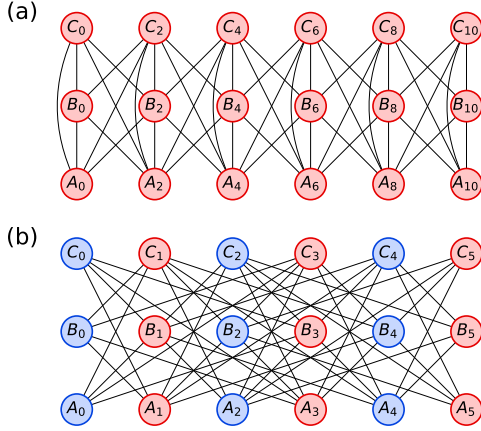


FIG. 6. Frustration graphs of the $\{A = X^{\otimes r}, B = Y^{\otimes r}, C = Z^{\otimes r}\}$ ensembles with (a) $r = 3$ and (b) $r = 4$, for a finite system. Each vertex represents one operator; edges connect anticommuting operators. For r odd, the graph decomposes into two identical, disconnected subgraphs – (a) shows only one of them. For r even, the graph is connected but bipartite (as indicated by the color scheme in (b)), which prevents a volume-law phase.

the ‘clipped gauge’⁴⁶, and find a power-law tail $P(\ell) \sim K\ell^{-2}$ as expected of a critical point, see Fig. 5. The coefficient K is found to increase with the effective range \tilde{r} of the bipartite ensembles. This is also related to the coefficient of the logarithm in the entropy, $S(\ell) \sim \frac{K}{2} \ln(\ell)$ (one bit of entropy is carried by *two* stabilizers straddling a boundary).

We conclude this discussion by noting that a bipartition in the frustration graph need not be between operator species. The ensembles $\{A = X^{\otimes r}, B = Y^{\otimes r}, C = Z^{\otimes r}\}$, for example, exhibit strikingly different behavior depending on whether r is even or odd – a volume-law phase is possible for odd r ($r > 1$), but not for even r , which is area-law or at most critical (depending on the probabilities $P_{A,B,C}$). As we have seen, the odd- r behavior (which admits a volume-law phase) is the generic one. The reason for the anomalous behavior at even r is that the frustration graph is bipartite *spatially*: all strings starting on even sites $\{A_{2j}, B_{2j}, C_{2j}\}$ commute amongst themselves; same for those starting on odd sites, $\{A_{2j+1}, B_{2j+1}, C_{2j+1}\}$. This is not true for odd r , where e.g. A_0, B_0 and C_0 anticommute pairwise and thus form a triangular subgraph; see Fig. 6.

This may also explain the critical behavior of the $r = 2$ factorizable ensemble studied in Fig. 4(b). While that ensemble is *not* bipartite, it appears to have the same critical behavior as the $\{XX, YY, ZZ\}$ ensemble, which is bipartite. Moreover, its entanglement immediately drops from logarithmic to area-law upon biasing the probability of measuring even and odd bonds (while it is robust to small changes in the \mathbf{q} parameters, as long as there is no bias between even and odd bonds). This indicates that a spatial bipartition is involved.

V. CRITICAL PROPERTIES

Having established the existence of entanglement phases in these models, it is interesting to ask whether the entanglement transitions are the same as those found in unitary-projective circuits^{46,55,56}. To address this question, we study the *tripartite mutual information*,

$$\mathcal{I}_3(A, B, C) = S(A) + S(B) + S(C) + S(A \cup B \cup C) - S(A \cup B) - S(B \cup C) - S(C \cup A)$$

evaluated for three consecutive intervals A, B, C of length $L/4$. This was found⁵⁴ to give a good estimate of the critical point due to its very limited finite-size drift at criticality (unlike the entanglement entropy, which drifts logarithmically). The single-parameter scaling ansatz

$$\mathcal{I}_3(q, L) \sim F[(q - q_c)L^{1/\nu}], \quad (17)$$

where q parametrizes the measurement ensemble, can be used to obtain the correlation length critical exponent ν .

We first consider the $r = 3$ factorizable model studied in Section IV A 2. Along the $q_Z = 0$ line, this has an area-to-volume critical point (shown by the star in Fig. 4(b)) at $q_{X,c} = 0.274(2)$. We note that this model, consisting of Pauli strings $\{XXX, XXY, \dots YYY\}$, has two independent ‘integrals of motion’, i.e. global Pauli strings which commute with all measurements⁸²: $\prod_j Z_{3j}Z_{3j+1}$ and $\prod_j Z_{3j+1}Z_{3j+2}$. These operators, which generically appear in the steady state in all phases, contribute two bits of *positive* tripartite mutual information \mathcal{I}_3 . This offsets the area-law value to $\mathcal{I}_3 = 2$, as seen in Fig. 7(a). In the vicinity of the critical point, the scaling ansatz Eq. (17) yields a good collapse with correlation length exponent $\nu = 1.1(1)$, as shown in Fig. 7(b). Additionally, we find that the entanglement entropy at the critical point obeys $S(\ell) \simeq K \ln \ell$ with $K = 1.0(1)$.

We also study the local order parameter introduced in Ref. [55], i.e. the long-time limit of the entanglement $S_R(t) \equiv S(\rho_R(t))$ of a reference qubit R initialized in a Bell pair state with a qubit at position x in the system. In the area-law (pure) phase S_R vanishes as the reference is quickly disentangled, while in the volume-law (mixed) phase entanglement persists for exponentially long times. At criticality S_R vanishes parametrically slowly in system size, $S_R(t) \sim G(t/L^z)$ for some function G . We find a dynamical exponent $z = 1$, in agreement with previous studies on the transition in unitary-projective circuits.

We repeat the same analysis for the l -bit inspired ensemble introduced in Section IV B. There, too, we find (see Fig. 8) a correlation length critical exponent $\nu = 1.1(1)$, consistent with the other model we discussed. The entanglement entropy at the critical point scales like $S(\ell) = K \ln \ell$ with $K = 0.8(1)$ and the dynamical exponent is again $z = 1$.

The critical properties of these two examples are compatible, pointing to the possibility of a unique universality class for measurement-only entanglement transitions.

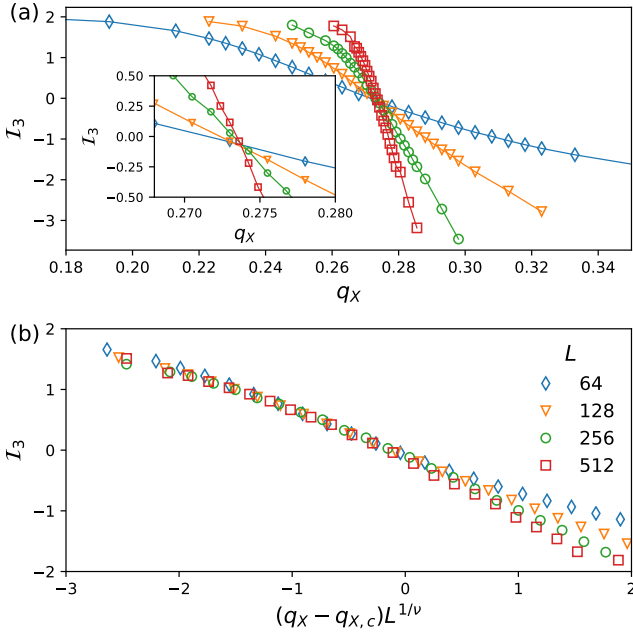


FIG. 7. Entanglement transition in the factorizable ensemble $q = (0, q_x, 1 - q_x, 0)$ with range $r = 3$. (a) Tripartite mutual information I_3 as a function of q_x . The value $I_3 = 2$ on the area-law side is due to the presence of two integrals of motion (bits of global entanglement). Different sizes $64 \leq L \leq 512$ show a crossing at $q_x = q_{x,c} = 0.274(2)$ (inset). (b) Scaling collapse of the data with exponent $\nu = 1.1$.

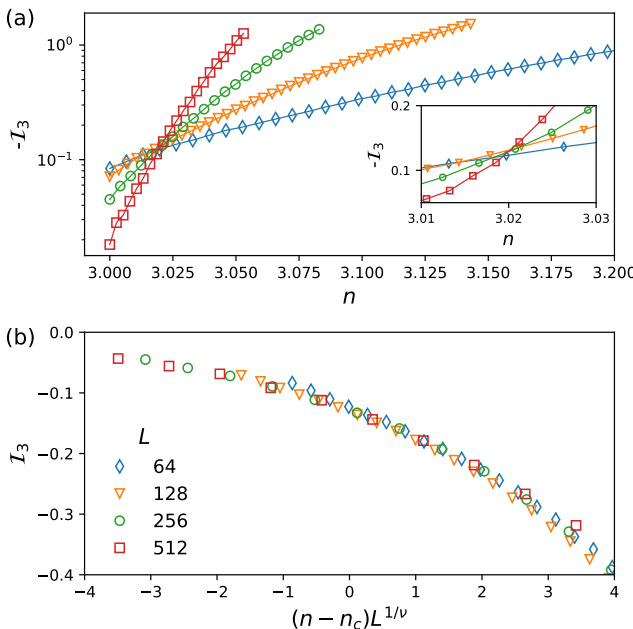


FIG. 8. Entanglement transition in the l -bit measurement-only model at “fractional n ” between 3 and 4. (a) Tripartite mutual information I_3 as a function of n . Different sizes $64 \leq L \leq 512$ show a crossing at $n = n_c = 3.020(3)$ (inset). (b) Scaling collapse of the data with exponent $\nu = 1.1$.

However, the limited resolution on the critical exponents (and the large variety of other models we have not studied) leave the door open to the existence of multiple universality classes. Hybrid unitary-projective circuits were found to have multiple universality classes (e.g. for Clifford and Haar-random gates), with quantitatively similar yet distinct exponents⁵⁶; an analogous scenario may hold here. A conclusive investigation of this issue is left for future work.

VI. LOCALITY AND INFORMATION SPREADING

The effect of local measurements on entangled states was famously described as a “spooky action at a distance”^{83,84}. In these models, where the entirety of the dynamics is made up of measurements on entangled states, there is good reason to expect spooky surprises. For instance, unlike local unitary circuits which have a strict light-cone, local projective measurements allow for the creation of arbitrary-range entanglement on an $O(1)$ timescale, using two layers of local measurements acting on a product state. One can see this as follows⁷⁴: Start from a Z -product state on a chain of length L , with tableau $\{g_i = Z_i : i = 1, \dots, L\}$. Measuring the operators $X_1 X_2, \dots, X_{L-1} X_L$ (all commuting, and thus measurable at the same time) creates a cluster state⁸⁵ spanning the entire chain; then, measuring operators Z_2, \dots, Z_{L-1} (again all commuting) yields a Bell pair shared between sites $(1, L)$. While fine-tuned (and thus unlikely to occur if the measurements are placed randomly in spacetime), this example shows that there is in general no strict light cone for the production of entanglement or correlations in this type of dynamics⁸⁶. Any emergent light cone must be statistical in nature – i.e., must reflect the fact that histories that produce entanglement outside the putative light cone are possible but rare.

The propagation of information in quantum systems is described by the spreading of local operators evolved in the Heisenberg picture^{5,26,27,87}. In the presence of measurements, the Heisenberg picture is problematic, since the Born probabilities needed to choose projectors must be computed on a state⁸⁸. Nevertheless, one can still ask how information spreads across the system. In what follows we propose a diagnostic for information spreading and verify the emergence of a statistical light-cone.

For concreteness we focus on Clifford circuits in what follows, but the ideas are straightforward to generalize. Consider entangling a reference qubit R to the center of the 1D chain at time $t = 0$, and running the measurement-only dynamics on the system. For concreteness, let us take a chain of odd length $L = 2l + 1$, with qubits numbered by $-l \leq n \leq l$, so that R is initially in a Bell-pair state with the qubit at $n = 0$. After a time t , R is either entangled with the system or not; in the volume law phase, it stays entangled with finite probability out to very long times. The entanglement be-

tween R and the system has previously been studied as an order parameter for the volume law phase. Crucially, if one assumes that there is a light-cone, R is entangled only with some interval of the system, $[-x, x]$. The size of this subsystem is what captures information spreading in this setting. One can estimate this by calculating the mutual information between R and segments of variable length centered at the point of initial entanglement, $[-x, x]$. This defines a function on spacetime,

$$f(x, t) = \mathcal{I}(R : [-x, x])|_t, \quad (18)$$

which quantifies how much information about the operators initially entangled with R (X_0 and Z_0 at $t = 0$) can be recovered by looking only at the region $[-x, x]$ at time t . Equal-value contours of $f(x, t)$ thus capture the spread of these operators.

At the initial time, we have $f(x, 0) = 2$ everywhere: any subsystem (as defined above) includes the central qubit. At late times, $f(L/2, t)$ is equal to the local order parameter $S_R(t)$ introduced in Ref. 55 and discussed in Sec. IV, which has a finite value in the volume-law phase. More precisely, we expect $f(x, t \gg L)$ to approach zero for $x < l/2$ and a finite constant for $x > l/2$ (where $L = 2l + 1$). This is because information hidden in a random state of L qubits is recoverable with high probability from any subsystem of more than $L/2$ qubits (a result that follows from the quantum channel capacity of the erasure channel^{89,90}). At intermediate times, we expect f to develop a ‘hole’ near $x = 0$ which progressively expands until eventually saturating to half the system. This expectation is borne out by numerics on the factorizable ensemble $q_X = q_Y = q_Z = 1/3$ at ranges $r = 3$ and 5 (see Fig. 9), where the operator spreading is found to be ballistic, with a ‘butterfly velocity’ v_B that increases with r .

Outside the volume-law phase, $f(x, t)$ decays in time for all values of x . It is nonetheless possible to define a normalized $\tilde{f}(x, t) \equiv f(x, t)/2S_R(t)$, where $2S_R(t) = f(L/2, t)$ is the mutual information between the reference R and the whole system, and analyze the information spreading in the same way as for the volume law phase (though in practice this makes the data considerably noisier). Fig. 9 includes data for the same factorizable ensemble with $r = 2$, which is critical. While the data is much noisier in this case (due to the majority of realizations becoming disentangled over short times and contributing no signal), it is clear that the spread of information is still bounded by a finite velocity. The infinite entanglement velocity identified in Ref.⁸⁶ for measurement-induced critical points is not seen through this diagnostic. While nonlocal creation of entanglement through processes such as the ‘entanglement swapping’ outlined above are likely happening, they seem to be statistically irrelevant to the dynamics of the encoded quantum information. For stabilizer circuits, the conditional trajectories where the reference qubit does not purify necessarily undergo purely unitary evolution, despite the nonunitary measurements. Our results shown

here indicate that this effective time-local random unitary evolution may also have a spatially local description throughout the phase diagram.

The application of this diagnostic to other models (both measurement-only and hybrid) is left for future work.

VII. DISCUSSION

The entanglement transition has been widely explained in terms of a competition between scrambling (which favors a volume law phase) and projective measurement (which favors an area law phase). In this work, by exploring systems in which scrambling is absent, we have shown that this understanding is incomplete: entanglement transitions can also arise in the absence of scrambling, provided that multi-site, incompatible (i.e., non-commuting) observables are measured. In the presence of multi-site incompatible measurements, a volume-law phase is in fact *generic*: one has to fine-tune the ensemble of measurements to achieve an area-law phase – the observables must either be very short ($r \lesssim 3$), very likely to commute, or meet a fine-tuned algebraic requirement (see Sec. IV C). This central result of our work is counterintuitive from the standard perspective, which suggests that the area-law phase should be generic when measurements dominate. A particularly striking consequence of our discussion is that many-body localized systems subject to projective measurements can have a stable volume-law phase: as we have seen (Fig. 2) this prediction is borne out numerically.

The volume-law phase that we have studied here is a potentially distinctive type of random quantum error-correcting code. An ensemble of measurements, implemented randomly, protects quantum information from *any* future sequence of randomly drawn measurements from that ensemble. This situation differs from prior studies of unitary-projective circuits, where the unitary evolution competes with the local measurements to hide quantum information in nonlocal degrees of freedom faster than it is measured. An interesting question, worth exploring in future work, is whether the properties of the volume law phase as a code differ in any qualitative respect between generic unitary-projective circuits and the measurement-only dynamics we have studied here. Often times in quantum computing devices, noise is not uniformly random, but has biases and correlations. By selecting the measurement ensemble to reflect the detailed properties of the noise, it may be possible to tailor codes for the specific noise configuration of the device⁹¹.

The quantum critical points we have found here raise many questions that we hope to address in future work. The critical exponents for the volume- to area-law transition appear different from those that were previously found in generic unitary-projective circuits, suggesting that these transitions might belong to a different universality class. More intensive numerical work needs to be

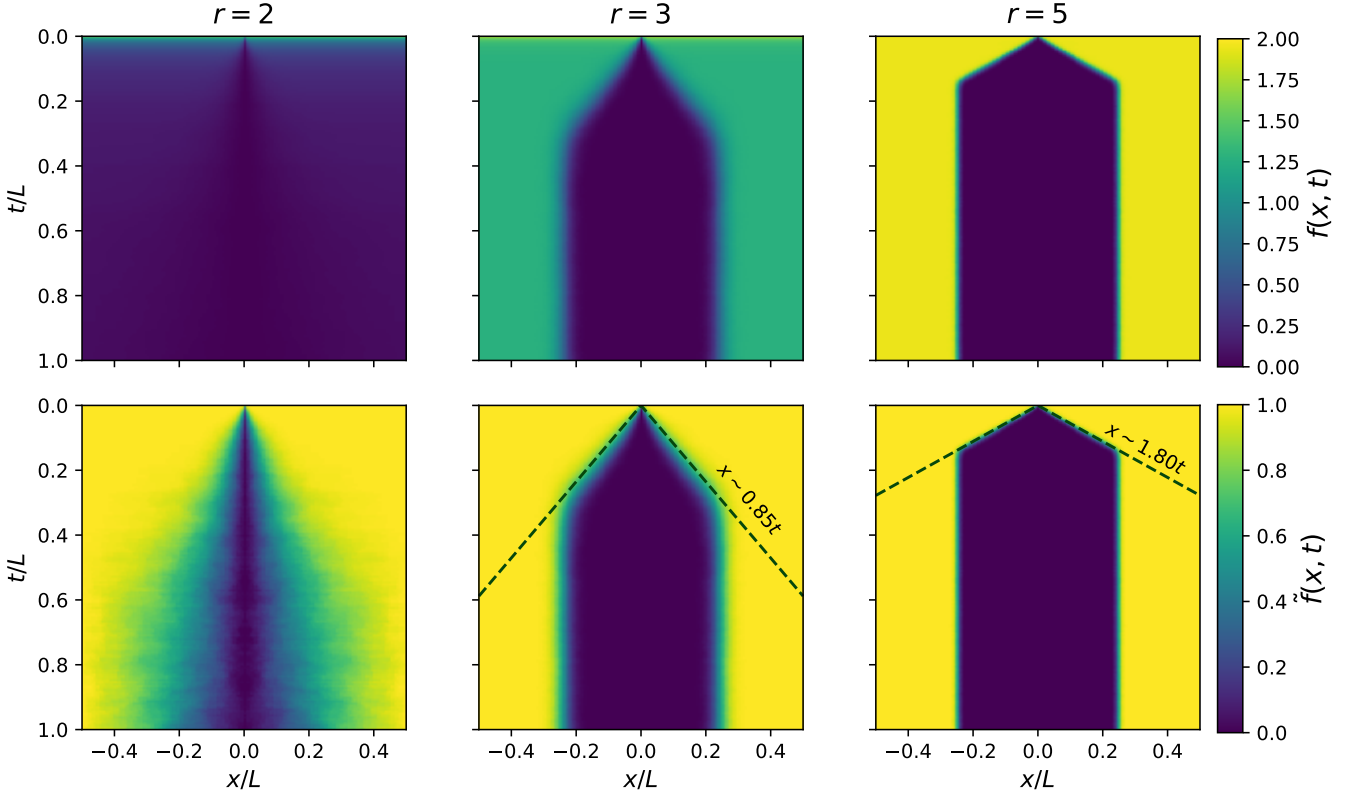


FIG. 9. Information spreading in measurement-only dynamics. Top: $f(x, t)$ as defined in Eq. (18) (mutual information between a reference initially entangled at $x = 0$ and a region $[-x, x]$) for factorizable ensembles $q = (0, 1/3, 1/3, 1/3)$ of range $r = 2$ (critical), 3 and 5 (volume-law). There is a clear ballistic light cone in the volume-law phase. The light cone saturates to half the system size. Bottom: the normalized quantity $\tilde{f}(x, t) = f(x, t)/2S_R(t)$ reveals a light cone in the critical phase as well. The approximate location of the wavefront is highlighted with a dashed line. The butterfly velocity $x \sim v_B t$ increases with increasing range r .

done to settle this question; adapting the construction of Ref. [92] to study these transitions, and exploring them away from the Clifford limit, would also be interesting extensions. In addition, we have found a critical phase as well as transitions between two area-law phases. These are reminiscent in some ways of the transitions found in free-fermion models in Ref. [80], which map to loop models; it would be interesting to understand whether the critical points we discovered admit loop model-based descriptions as well.

ACKNOWLEDGMENTS

We thank Roderich Moessner, Jed Pixley, Romain Vasseur, Dominic Williamson, Justin Wilson and Aidan Zabalo for insightful discussions and collaborations on related topics. This work was supported with funding from the Defense Advanced Research Projects Agency (DARPA) via the DRINQS program. The views, opinions and/or findings expressed are those of the authors and should not be interpreted as representing the official views or policies of the Department of Defense or

the U.S. Government. M.I. was funded in part by the Gordon and Betty Moore Foundation’s EPiQS Initiative through Grant GBMF4302 and GBMF8686. S.G. acknowledges support from NSF DMR-1653271. D.A.H. was also supported in part by a Simons Fellowship.

Appendix A: Details on stabilizer dynamics

Here we review the stabilizer formalism for Pauli measurements to complement the brief discussion in Sec. III B. Let us consider a stabilizer state as in Eq. (5), starting from the case of a pure state, $s = L$. The stabilizer tableau \mathcal{T} , as defined in Eq. (6), is a $L \times 2L$ matrix with full rank (L) over \mathbb{Z}_2 . Under Clifford unitaries and Pauli measurements, \mathcal{T} can be updated in polynomial time with operations that amount to linear algebra over \mathbb{Z}_2 ⁹³. In the following we use ‘tableau’ somewhat flexibly to refer to either the matrix \mathcal{T} or a list of stabilizer generators $\{g_i\}$; the two notions are always related via Eq. (6).

The key idea is that all stabilizers in the tableau must commute with one another, $[g_i, g_j] = 0$ (as it is impos-

sible for two anticommuting operators to share a $+1$ eigenstate); therefore, when measuring a new operator O , three possibilities arise:

1. O commutes with all rows of \mathcal{T} . This guarantees that O can be written as a product of g_i 's (up to a sign). The measurement outcome is deterministic and the state is unchanged by the measurement.
2. O anticommutes with exactly one row in \mathcal{T} , say g_1 . The measurement outcome is $s = \pm 1$ chosen randomly; g_1 is updated to $g'_1 = sO$.
3. O anticommutes with several rows, say rows 1 through k . This case can always be reduced to the previous one by a gauge transformation, i.e. a sequence of invertible row transformations in \mathcal{T} (for example $g'_i = g_i g_1$ for all $1 < i \leq k$, after which only g_1 anticommutes with O).

It can also be useful to adopt the ‘purification’ point of view⁵⁴, where one starts with a mixed stabilizer state (Eq. (5) with $s < L$) represented by an incomplete tableau $\{g_i : i = 1, \dots, s\}$, possibly the empty tableau $\{\}$ for the maximally mixed state $\rho = \mathbb{I}/2^L$ ($s = 0$). In the volume-law phase the state remains mixed for exponentially long times, whereas in the area-law phase the state becomes pure in time $\text{poly}(L)$. The entanglement transition thus corresponds to a purification transition. In this mixed-state scenario, processes 2 and 3 play out in the same way, but process 1 must be subdivided into

- 1A. O commutes with all rows in \mathcal{T} but is *not* part of the stabilizer group (i.e., cannot be written as a product of the $\{g_i\}$). The measurement outcome is $s = \pm 1$, chosen at random, and a new row $g_{r+1} = sO$ is added to the tableau. The state gains one bit of purity ($r \mapsto r + 1$).
- 1B. O commutes with all rows in \mathcal{T} and is part of the stabilizer group (up to a sign). The measurement outcome is deterministic, and the state is unchanged by the measurement.

Appendix B: Details on the frustration tensor

In this Appendix we prove some additional properties of the frustration tensor, Eq. (7), completing the discussion in Sec. III D.

1. Simulation of the dynamics

The stabilizer tableau update rules reviewed in Sec. III B and Appendix A never involve the operators O_α directly, but only their anticommutation and algebraic dependence properties. Given these data, one can forget the specific form of the operators O_α and simulate the dynamics blindly, as we prove in the following.

Consider measuring an operator $O_{\alpha,n}$. To update the tableau \mathcal{T} , we must first test the commutation between this and the existing rows. This only requires knowledge of the frustration tensor $\Gamma_\ell^{\alpha\beta}$. Indeed, let us decompose each row of \mathcal{T} as (up to a phase)

$$g_i = \prod_{\alpha,n} O_{\alpha,n}^{v_{\alpha,n}^i} \quad (\text{B1})$$

for appropriate coefficients $v_{\alpha,n}^i \in \mathbb{Z}_2$, not necessarily unique (such a decomposition is known, trivially, for the maximally mixed state $\rho \propto \mathbb{I}$, and can be consistently obtained without direct knowledge of the O_α , as we will show). $O_{\alpha,n}$ and g_i commute if and only if

$$O_{\alpha,n} \circ g_i = \sum_{\beta,n'} \Gamma_{n-n'}^{\alpha\beta} v_{\beta,n'}^i \equiv 0 \pmod{2}.$$

Any anticommuting rows can be dealt with according to cases 2-3 in Appendix A. If there are no anticommuting rows (case 1), we consider adding the newly measured $O_{\alpha,n}$ to the tableau. This would be a new stabilizer g_i parametrized as in Eq. (B1) with $v_{\beta,n'}^i = \delta_{n,n'} \delta_{\alpha,\beta}$. Deciding whether this new row is added to \mathcal{T} (case 1A) or not (case 1B) in general requires knowledge of all algebraic dependence relations between the operators $\{O_{\alpha,n}\}$. Absent any such relations (typically the case for two independent operator species), this is just linear independence of the new row v^i on all existing rows in \mathcal{T} . If algebraic relations are present (typically for 3 or more species), one can express any operator in terms of two independent species A, B as

$$O_{\gamma,n} = \prod_{\ell,\ell'} O_{A,n+\ell}^{f_\ell^{A\gamma}} O_{B,n+\ell'}^{f_{\ell'}^{B\gamma}}$$

in terms of suitable coefficients $f_\ell^{\alpha\gamma} \in \mathbb{Z}_2$, where α ranges over the independent species A, B and γ ranges over all other dependent species. Then one can define a tableau \tilde{v} in terms of only the independent species,

$$\tilde{v}_{A,n}^i \equiv v_{A,n}^i + \sum_{\gamma,\ell} f_\ell^{A\gamma} v_{\gamma,n+\ell}^i,$$

and similarly for $\tilde{v}_{B,n}^i$. Algebraic independence is thus mapped to linear independence of the \tilde{v}^i rows.

In conclusion, all the data needed to update the tableau for a given measurement is contained in the frustration tensor $\Gamma_\ell^{\alpha\beta}$ and any algebraic dependence relations $f_\ell^{(A/B)\gamma}$. None of this requires explicit knowledge of the $\{O_{\alpha,n}\}$ operators. Entanglement calculations in general require us to transform the stabilizer generators g back to the physical basis of $\{X_n, Z_n\}$. However this is not necessary to decide the entanglement *phase*: in the purification picture this is decided simply by counting the rows in the tableau at late times (L rows in the area-law phase, fewer than L in the volume-law phase). This shows that the dynamics can be simulated using

only the frustration tensor $\Gamma_\ell^{\alpha\beta}$, the species probability distribution P_α , and any algebraic dependence between the $O_{\alpha,n}$.

2. Equivalence between ensembles

If two ensembles \mathcal{E} and \mathcal{E}' have frustration graphs that can be transformed into one another by moving vertices around without breaking or creating any edges, then there is a mapping $O_{\alpha,n} \leftrightarrow O'_{\beta,m}$ between the operators in the two ensembles which preserves all commutation relations. If the probability distributions are invariant under this mapping as well (as is always the case for the uniform distribution), then the dynamics induced by \mathcal{E} and \mathcal{E}' are in fact equivalent, and the two ensembles are in the same phase.

Among the applications of these graph-theoretic ideas is a method to determine whether an ensemble is equivalent to free fermion measurements⁷⁵. For free fermion ensembles, the frustration graph is a ‘line graph’: there exists another graph whose vertices are Majorana fermions and whose edges are the ensemble operators. The property of being a line graph can be tested in time $O(L)$ in the general case, and in time $O(r)$ for our local (range r), translationally-invariant models.

Aside from mappings to free fermions, graph equivalence allows us to prove that seemingly distinct ensembles belong to the same phase, or even more detailed relations between their steady-state entanglement entropy. As an example, we show in Fig. 10 that the ensembles $\mathcal{E}_1 = \{X_0X_1X_2, Z_0Z_1Z_2\}$, $\mathcal{E}_2 = \{X_1, Z_0Z_1Z_2\}$ and $\mathcal{E}_3 = \{X_0Z_1, Z_0Y_1\}$ (with the two species sampled uniformly in all cases) are all in the same phase: the graph for \mathcal{E}_1 splits into two subgraphs, each of which is equivalent to \mathcal{E}_2 ; additionally, \mathcal{E}_2 and \mathcal{E}_3 are equivalent to each other.

3. Frustration profile of factorizable ensembles

Here we provide a derivation of the result Eq. (10) on the frustration profile (i.e. species-averaged frustration tensor) of factorizable ensembles, Sec. IV A. Let us start from a displacement of $\ell = r - 1$, i.e. Pauli strings overlapping on a single site. The probability that they anticommute is by definition $\bar{\Gamma}_{r-1}$. Letting $\bar{\Gamma}_{r-1} = \chi$ for future convenience, we have

$$\chi = 2(q_X q_Y + q_Y q_Z + q_Z q_X) = 2\mathbf{q} \cdot R_{2\pi/3}^{(111)} \mathbf{q},$$

where $\mathbf{q} = (q_X, q_Y, q_Z)$ and $R_\theta^{(111)}$ is a rotation about the (111) axis in \mathbf{q} space. Decomposing $\mathbf{q} = \mathbf{q}_\parallel + \mathbf{q}_\perp$, with $\mathbf{q}_\parallel = (1, 1, 1)/3$ (fixed by the normalization of probabilities) and $\mathbf{q}_\perp \cdot \mathbf{q}_\parallel = 0$, we obtain

$$\chi = 2q_\parallel^2 + 2q_\perp^2 \cos \frac{2\pi}{3} = \frac{2}{3} - q_\perp^2,$$

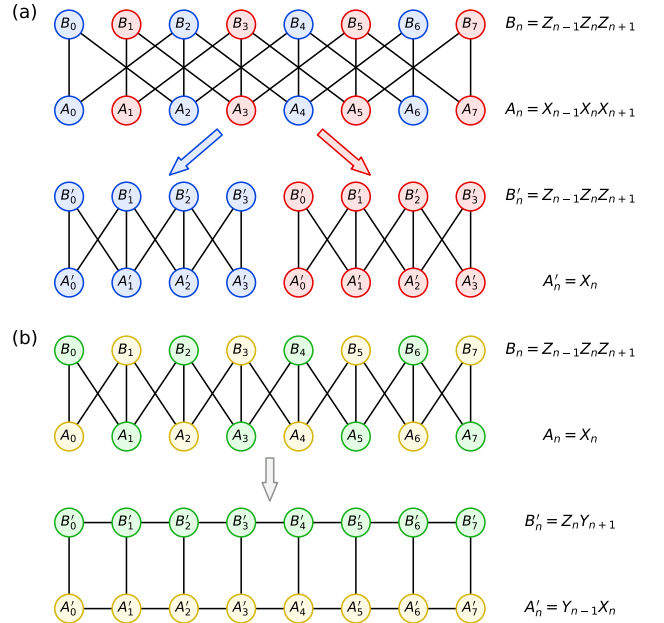


FIG. 10. Dualities revealed by graph equivalence. (a) The frustration graph for the ensemble $\mathcal{E}_1 = \{Z_0Z_1Z_2, X_0X_1X_2\}$ has two connected components, highlighted by the color scheme. Separating the two yields two copies of ensemble $\mathcal{E}_2 = \{Z_0Z_1Z_2, X_1\}$. (b) The ensemble \mathcal{E}_2 is in turn equivalent to $\mathcal{E}_3 = \{Z_0Y_1, Y_0X_1\}$ via a permutation of vertices, as highlighted by the color scheme.

hence the center of the triangle ($q_\perp = 0$) is the maximally anticommuting point, and contours of ‘equal commutativity’ are circular. Values of $\bar{\Gamma}_\ell$ for $\ell < r - 1$ are found recursively: $\bar{\Gamma}_{r-k}$ is the probability that two strings overlapping on k sites anticommute; splitting the overlapping region into two intervals of length $k - 1$ and 1 gives

$$\begin{aligned} \bar{\Gamma}_{r-k} &= \bar{\Gamma}_{r-1}(1 - \bar{\Gamma}_{r-k+1}) + \bar{\Gamma}_{r-k+1}(1 - \bar{\Gamma}_{r-1}) \\ &= \bar{\Gamma}_{r-k+1}(1 - 2\chi) + \chi, \end{aligned}$$

and the geometric series

$$\frac{1}{2} - \bar{\Gamma}_{r-k} = (1 - 2\chi) \left(\frac{1}{2} - \bar{\Gamma}_{r-k+1} \right),$$

which finally yields Eq. (10). On the $q_\perp = 1/\sqrt{6}$ circumference, which is tangent to the sides of the triangular \mathbf{q}_\perp parameter space, the frustration profile is box-shaped, $\bar{\Gamma}_\ell = \frac{1}{2}\Theta(r - \ell)$. Outside this circumference $\bar{\Gamma}_\ell$ is monotonically decreasing; inside of it (including the center $q_\perp = 0$) it shows even-odd oscillations with ℓ .

¹ A. Polkovnikov, K. Sengupta, A. Silva, and M. Vengalattore, Rev. Mod. Phys. **83**, 863 (2011).

² D. M. Basko, I. L. Aleiner, and B. L. Altshuler, Ann. Phys. (Amsterdam) **321**, 1126 (2006).

³ R. Nandkishore and D. A. Huse, Annual Review of Condensed Matter Physics **6**, 15 (2015), <https://doi.org/10.1146/annurev-conmatphys-031214-014726>.

⁴ D. A. Abanin, E. Altman, I. Bloch, and M. Serbyn, Rev. Mod. Phys. **91**, 021001 (2019).

⁵ J. Maldacena, S. H. Shenker, and D. Stanford, Journal of High Energy Physics **2016**, 106 (2016).

⁶ L. D’Alessio, Y. Kafri, A. Polkovnikov, and M. Rigol, Advances in Physics **65**, 239 (2016), <https://doi.org/10.1080/00018732.2016.1198134>.

⁷ N. Shiraishi and T. Mori, Phys. Rev. Lett. **119**, 030601 (2017).

⁸ S. Moudgalya, N. Regnault, and B. A. Bernevig, Phys. Rev. B **98**, 235156 (2018).

⁹ C. J. Turner, A. A. Michailidis, D. A. Abanin, M. Serbyn, and Z. Papic, Nature Physics **14**, 745 (2018).

¹⁰ S. Choi, C. J. Turner, H. Pichler, W. W. Ho, A. A. Michailidis, Z. Papić, M. Serbyn, M. D. Lukin, and D. A. Abanin, Phys. Rev. Lett. **122**, 220603 (2019).

¹¹ V. Khemani, R. Moessner, and S. Sondhi, arXiv e-prints, arXiv:1910.10745 (2019).

¹² F. Harper, R. Roy, M. S. Rudner, and S. Sondhi, Annu. Rev. Condens. Matter Phys. **11** (2020).

¹³ P. Calabrese and J. Cardy, Journal of Statistical Mechanics: Theory and Experiment **2005**, P04010 (2005).

¹⁴ M. Žnidarič, T. c. v. Prosen, and P. Prelovšek, Phys. Rev. B **77**, 064426 (2008).

¹⁵ J. H. Bardarson, F. Pollmann, and J. E. Moore, Phys. Rev. Lett. **109**, 017202 (2012).

¹⁶ T. Hartman and J. Maldacena, Journal of High Energy Physics **2013**, 14 (2013).

¹⁷ H. Liu and S. J. Suh, Phys. Rev. Lett. **112**, 011601 (2014).

¹⁸ H. Kim and D. A. Huse, Phys. Rev. Lett. **111**, 127205 (2013).

¹⁹ R. Islam, R. Ma, P. M. Preiss, M. E. Tai, A. Lukin, M. Rispoli, and M. Greiner, Nature **528**, 77 (2015).

²⁰ A. M. Kaufman, M. E. Tai, A. Lukin, M. Rispoli, R. Schittko, P. M. Preiss, and M. Greiner, Science **353**, 794 (2016).

²¹ M. Mezei and D. Stanford, Journal of High Energy Physics **2017**, 65 (2017).

²² A. Nahum, J. Ruhman, S. Vijay, and J. Haah, Phys. Rev. X **7**, 031016 (2017).

²³ V. Alba and P. Calabrese, Proceedings of the National Academy of Sciences **114**, 7947 (2017).

²⁴ T. Rakovszky, F. Pollmann, and C. W. von Keyserlingk, Phys. Rev. Lett. **122**, 250602 (2019).

²⁵ Y. Huang, arXiv preprint arXiv:1902.00977 (2019).

²⁶ A. Nahum, S. Vijay, and J. Haah, Phys. Rev. X **8**, 021014 (2018).

²⁷ C. W. von Keyserlingk, T. Rakovszky, F. Pollmann, and S. L. Sondhi, Phys. Rev. X **8**, 021013 (2018).

²⁸ T. Rakovszky, F. Pollmann, and C. W. von Keyserlingk, Phys. Rev. X **8**, 031058 (2018).

²⁹ V. Khemani, D. A. Huse, and A. Nahum, Phys. Rev. B **98**, 144304 (2018).

³⁰ A. Nahum, J. Ruhman, and D. A. Huse, Phys. Rev. B **98**, 035118 (2018).

³¹ A. Chan, A. De Luca, and J. T. Chalker, Phys. Rev. X **8**, 041019 (2018).

³² J. Preskill, Quantum **2**, 79 (2018).

³³ F. Arute, K. Arya, R. Babbush, D. Bacon, J. C. Bardin, R. Barends, R. Biswas, S. Boixo, F. G. S. L. Brandao, D. A. Buell, B. Burkett, Y. Chen, Z. Chen, B. Chiaro, R. Collins, W. Courtney, A. Dunsworth, E. Farhi, B. Foxen, A. Fowler, C. Gidney, M. Giustina, R. Graff, K. Guerin, S. Habegger, M. P. Harrigan, M. J. Hartmann, A. Ho, M. Hoffmann, T. Huang, T. S. Humble, S. V. Isakov, E. Jeffrey, Z. Jiang, D. Kafri, K. Kechedzhi, J. Kelly, P. V. Klimov, S. Knysh, A. Korotkov, F. Kostritsa, D. Landhuis, M. Lindmark, E. Lucero, D. Lyakh, S. Mandrà, J. R. McClean, M. McEwen, A. Megrant, X. Mi, K. Michelsen, M. Mohseni, J. Mutus, O. Naaman, M. Neeley, C. Neill, M. Y. Niu, E. Ostby, A. Petukhov, J. C. Platt, C. Quintana, E. G. Rieffel, P. Roushan, N. C. Rubin, D. Sank, K. J. Satzinger, V. Smelyanskiy, K. J. Sung, M. D. Trevithick, A. Vainsencher, B. Villalonga, T. White, Z. J. Yao, P. Yeh, A. Zalcman, H. Neven, and J. M. Martinis, Nature **574**, 505 (2019).

³⁴ D. Marolf, Reports on Progress in Physics **80**, 092001 (2017).

³⁵ P. Hayden and J. Preskill, J. High Energ. Phys. **2007**, 120 (2007), arXiv:0708.4025.

³⁶ L. Piroli, C. Sünderhauf, and X.-L. Qi, Journal of High Energy Physics **2020**, 63 (2020).

³⁷ K. Agarwal and N. Bao, arXiv preprint arXiv:1912.09491 (2019).

³⁸ R. Horodecki, P. Horodecki, M. Horodecki, and K. Horodecki, Rev. Mod. Phys. **81**, 865 (2009).

³⁹ C. B. Chiu, E. C. G. Sudarshan, and B. Misra, Phys. Rev. D **16**, 520 (1977).

⁴⁰ W. M. Itano, D. J. Heinzen, J. J. Bollinger, and D. J. Wineland, Phys. Rev. A **41**, 2295 (1990).

⁴¹ S. Diehl, A. Micheli, A. Kantian, B. Kraus, H. Büchler, and P. Zoller, Nature Physics **4**, 878 (2008).

⁴² F. Verstraete, M. M. Wolf, and J. I. Cirac, Nature physics **5**, 633 (2009).

⁴³ H. Fröml, A. Chiocchetta, C. Kollath, and S. Diehl, Phys. Rev. Lett. **122**, 040402 (2019).

⁴⁴ J. Dalibard, Y. Castin, and K. Mølmer, Physical review letters **68**, 580 (1992).

⁴⁵ H. Pichler, A. J. Daley, and P. Zoller, Phys. Rev. A **82**, 063605 (2010).

⁴⁶ Y. Li, X. Chen, and M. P. A. Fisher, Phys. Rev. B **98**, 205136 (2018).

⁴⁷ B. Skinner, J. Ruhman, and A. Nahum, Phys. Rev. X **9**, 031009 (2019).

⁴⁸ A. Chan, R. M. Nandkishore, M. Pretko, and G. Smith, Phys. Rev. B **99**, 224307 (2019).

⁴⁹ Y. Li, X. Chen, and M. P. A. Fisher, Phys. Rev. B **100**, 134306 (2019).

⁵⁰ V. Coffman, J. Kundu, and W. K. Wootters, Phys. Rev. A **61**, 052306 (2000).

⁵¹ S. Choi, Y. Bao, X.-L. Qi, and E. Altman, arXiv e-prints, arXiv:1903.05124 (2019), arXiv:1903.05124 [quant-ph].

⁵² Y. Bao, S. Choi, and E. Altman, Phys. Rev. B **101**, 104301 (2020).

⁵³ W. Brown and O. Fawzi, 2013 IEEE International Symposium on Information Theory, Istanbul , 346 (2013).

⁵⁴ M. J. Gullans and D. A. Huse, arXiv e-prints , arXiv:1905.05195 (2019), arXiv:1905.05195 [quant-ph].

⁵⁵ M. J. Gullans and D. A. Huse, arXiv e-prints , arXiv:1910.00020 (2019), arXiv:1910.00020 [cond-mat.stat-mech].

⁵⁶ A. Zabalo, M. J. Gullans, J. H. Wilson, S. Gopalakrishnan, D. A. Huse, and J. H. Pixley, Phys. Rev. B **101**, 060301 (2020).

⁵⁷ B. Swingle and D. Chowdhury, Phys. Rev. B **95**, 060201 (2017).

⁵⁸ Y. Huang, Y.-L. Zhang, and X. Chen, Annalen der Physik **529**, 1600318 (2017).

⁵⁹ Y. Chen, arXiv preprint arXiv:1608.02765 (2016).

⁶⁰ X. Chen, T. Zhou, D. A. Huse, and E. Fradkin, Annalen der Physik **529**, 1600332 (2017).

⁶¹ R. Fan, P. Zhang, H. Shen, and H. Zhai, Science bulletin **62**, 707 (2017).

⁶² R.-Q. He and Z.-Y. Lu, Phys. Rev. B **95**, 054201 (2017).

⁶³ M. A. Nielsen, Physics Letters A **308**, 96 (2003).

⁶⁴ H. J. Briegel, D. E. Browne, W. Dür, R. Raussendorf, and M. Van den Nest, Nature Physics **5**, 19 (2009).

⁶⁵ A. I. Larkin and Y. N. Ovchinnikov, Sov. Phys. JETP **28**, 1200 (1969).

⁶⁶ M. Serbyn, Z. Papić, and D. A. Abanin, Phys. Rev. Lett. **110**, 260601 (2013).

⁶⁷ D. A. Huse, R. Nandkishore, and V. Oganesyan, Phys. Rev. B **90**, 174202 (2014).

⁶⁸ M. Serbyn, Z. Papić, and D. A. Abanin, Phys. Rev. Lett. **111**, 127201 (2013).

⁶⁹ J. Z. Imbrie, Phys. Rev. Lett. **117**, 027201 (2016).

⁷⁰ D. K. Burgarth, P. Facchi, V. Giovannetti, H. Nakazato, S. Pascazio, and K. Yuasa, Nature Communications **5**, 5173 (2014).

⁷¹ S. Pouyandeh, F. Shahbazi, and A. Bayat, Phys. Rev. A **90**, 012337 (2014).

⁷² W.-L. Ma, P. Wang, W.-H. Leong, and R.-B. Liu, Phys. Rev. A **98**, 012117 (2018).

⁷³ D. Gottesman and I. L. Chuang, Nature **402**, 390 (1999).

⁷⁴ M. Żukowski, A. Zeilinger, M. A. Horne, and A. K. Ekert, Phys. Rev. Lett. **71**, 4287 (1993).

⁷⁵ A. Chapman and S. T. Flammia, arXiv e-prints , arXiv:2003.05465 (2020), arXiv:2003.05465 [quant-ph].

⁷⁶ M. Planat and M. Saniga, Quantum Information and Computation **8**, 127 (2007).

⁷⁷ A. Zhao, A. Tranter, W. M. Kirby, S. F. Ung, A. Miyake, and P. Love, arXiv e-prints , arXiv:1908.08067 (2019), arXiv:1908.08067 [quant-ph].

⁷⁸ P. Gokhale, O. Angiuli, Y. Ding, K. Gui, T. Tomesh, M. Suchara, M. Martonosi, and F. T. Chong, arXiv e-prints , arXiv:1907.13623 (2019), arXiv:1907.13623 [quant-ph].

⁷⁹ X. Cao, A. Tilloy, and A. D. Luca, SciPost Phys. **7**, 24 (2019).

⁸⁰ A. Nahum and B. Skinner, arXiv e-prints , arXiv:1911.11169 (2019), arXiv:1911.11169 [cond-mat.stat-mech].

⁸¹ A. Lavasani, Y. Alavirad, and M. Barkeshli, arXiv e-prints , arXiv:2004.07243 (2020), arXiv:2004.07243 [quant-ph].

⁸² For a finite system with periodic boundary conditions, this is true only if L is multiple of 3. We use open boundary conditions in this calculation.

⁸³ A. Einstein, B. Podolsky, and N. Rosen, Phys. Rev. **47**, 777 (1935).

⁸⁴ A. Einstein, in *The Born-Einstein Letters; Correspondence between Albert Einstein and Max and Hedwig Born from 1916 to 1955*, edited by B. M. Walker (Macmillan, New York, 1971) pp. 157–158.

⁸⁵ H. J. Briegel and R. Raussendorf, Phys. Rev. Lett. **86**, 910 (2001).

⁸⁶ Y. Li, X. Chen, A. W. W. Ludwig, and M. P. A. Fisher, arXiv e-prints , arXiv:2003.12721 (2020), arXiv:2003.12721 [quant-ph].

⁸⁷ B. Swingle, G. Bentsen, M. Schleier-Smith, and P. Hayden, Phys. Rev. A **94**, 040302 (2016).

⁸⁸ This is not an issue when averaging over measurement outcomes, in which case the adjoint of the quantum channel describing the (mixed) state evolution is perfectly well defined. Operator spreading in open systems was previously studied in Refs. 94–97.

⁸⁹ P. Hayden and J. Preskill, Journal of High Energy Physics **2007**, 120 (2007).

⁹⁰ C. H. Bennett, D. P. DiVincenzo, and J. A. Smolin, Phys. Rev. Lett. **78**, 3217 (1997).

⁹¹ D. K. Tuckett, A. S. Darmawan, C. T. Chubb, S. Bravyi, S. D. Bartlett, and S. T. Flammia, Phys. Rev. X **9**, 041031 (2019).

⁹² C.-M. Jian, Y.-Z. You, R. Vasseur, and A. W. W. Ludwig, arXiv e-prints , arXiv:1908.08051 (2019), arXiv:1908.08051 [cond-mat.stat-mech].

⁹³ S. Aaronson and D. Gottesman, Phys. Rev. A **70**, 052328 (2004).

⁹⁴ B. Swingle and N. Yunger Halpern, Phys. Rev. A **97**, 062113 (2018).

⁹⁵ Y.-L. Zhang, Y. Huang, and X. Chen, Phys. Rev. B **99**, 014303 (2019).

⁹⁶ M. J. Klug and S. V. Syzranov, Phys. Rev. B **100**, 094304 (2019).

⁹⁷ J. Tuziemski, Phys. Rev. A **100**, 062106 (2019).